ACS APPLIED MATERIALS & INTERFACES

Research Article

www.acsami.org

Synthesis of Few-Layered Graphene Nanoballs with Copper Cores Using Solid Carbon Source

Sanggeun Lee,[†] Juree Hong,[†] Ja Hoon Koo,[†] Hyonik Lee,[†] Seulah Lee,[†] Taejin Choi,[‡] Hanearl Jung,[‡] Bonwoong Koo,[§] Jusang Park,[‡] Hyungjun Kim,[‡] Young-Woon Kim,[§] and Taeyoon Lee[†,*]

[†]Nanobio Device Laboratory, School of Electrical and Electronic Engineering and [‡]Nanodevice Laboratory, School of Electrical and Electronic Engineering, Yonsei University, 50 Yonsei-ro, Seodaemun-Gu, Seoul 120-749, Republic of Korea

[§]in situ Electron Microscopy Laboratory, Department of Materials Science and Engineering, Seoul National University, 599 Gwanak-ro, Gwanak-Gu, Seoul, 31-411, Republic of Korea

Supporting Information

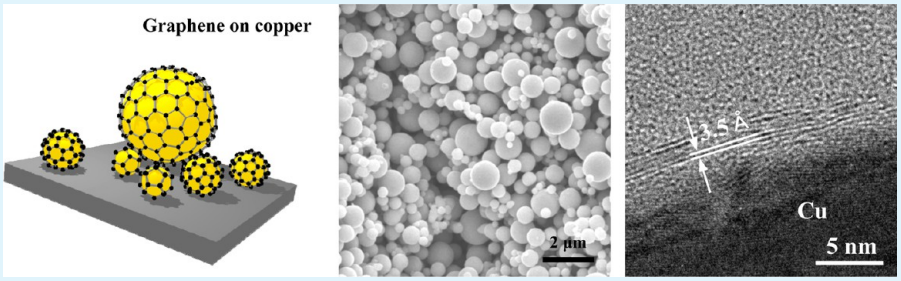

ABSTRACT: We report the fabrication of graphene-encapsulated nanoballs with copper nanoparticle (Cu NP) cores whose size range from 40 nm to 1 μm using a solid carbon source of poly(methyl methacrylate) (PMMA). The Cu NPs were prone to agglomerate during the annealing process at high temperatures of 800 to 900 °C when gas carbon source such as methane was used for the growth of graphene. On the contrary, the morphologies of the Cu NPs were unchanged during the growth of graphene at the same temperature range when PMMA coating was used. The solid source of PMMA was first converted to amorphous carbon layers through a pyrolysis process at the temperature regime of 400 °C, which prevented the Cu NPs from agglomeration, and they were converted to few-layered graphene (FLG) at the elevated temperatures. Raman and transmission electron microscope analyses confirmed the synthesis of FLG with thickness of approximately 3 nm directly on the surface of the Cu NPs. X-ray diffraction and X-ray photoelectron spectroscopy analyses, along with electrical resistance measurement according to temperature changes showed that the FLG-encapsulated Cu NPs were highly resistant to oxidation even after exposure to severe oxidation conditions.

KEYWORDS: *graphene, copper nanoparticle, encapsulation, graphene nanoball*

1. INTRODUCTION

Metal nanoparticles (NPs) have attracted unprecedented interests for the past few decades because of their unique and tunable electrical, optical, and mechanical properties according to the size, shape, and aggregation state, which could be suitable in various applications ranging from bioanalytical tools[1] to conductive inks for inkjet printing.[2] In particular, the use of noble metals such as gold,[3] silver,[2] and platinum[4] has been actively researched due to their excellent nonoxidizing properties and high conductivity. However, the high cost of such noble metals limited their use in widespread practical applications, which in turn created the demand for the synthesis of non-noble metal NPs that exhibit superior oxidation resistivity and electrical properties. In this respect, copper (Cu) NPs have been considered as a promising candidate that can replace the noble metal NPs since their fundamental material properties and processing have been already researched extensively.

Cu NPs can be fabricated with relatively low cost and they exhibit high electrical conductivity. Nonetheless, the poor oxidation resistance of the Cu NPs has hindered their use in practical applications; it is known that bare Cu NPs exposed in air ambient at room temperature were easily oxidized to form copper oxides within a few hours.[5] The formation of copper oxides not only leads to a severe degradation in the electrical conductivity,[6] but also induces undesirable shifts in the energy of surface plasmon resonance peaks.[7] Furthermore, the biocompatibility of copper oxides has been reported to be much worse than those of other non-noble metal NPs.[8] Thus, the poor oxidation resistance of the Cu NPs must be improved, and encapsulation of the Cu NPs by proper materials could be a possible solution to avoid the oxidation-related drawbacks.[6]

Received: October 29, 2012
Accepted: March 6, 2013
Published: March 6, 2013

dx.doi.org/10.1021/am3024965 | *ACS Appl. Mater. Interfaces* 2013, 5, 2432−2437

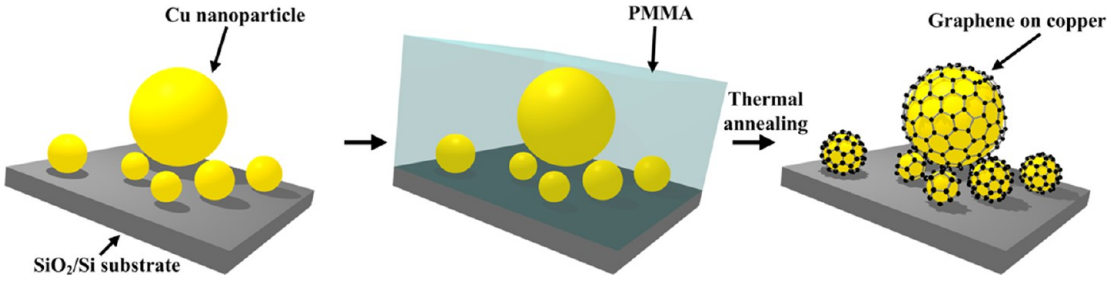

Figure 1. Fabrication process of GNBs using a solid carbon source (PMMA).

Graphene could be one of the ideal materials of choice for the encapsulation of Cu NPs owing to its exceptional electrical conductivity,[9] chemical stability,[10] and impermeability even to helium atoms.[11] However, not much has been reported on the methods to successfully synthesize graphene layers on Cu NPs, especially on Cu NPs with variable shapes and sizes. In the articles of Luechinger et al.[12] and Athanassiou et al.,[13] the reactive surfaces of Cu NPs were capped with few layers of graphene using flame synthesis, and verified that the thermal stability and electrical conductivity of the Cu NPs were enhanced after encapsulation with graphene layers. Recently, Wang et al.[14] reported the encapsulation of Cu NPs with few layers of graphene using metal−organic precursors containing both Cu and carbon (C) during the chemical vapor deposition (CVD) process; they showed that Cu NPs were highly resistive to oxidation, of which no sign of oxidation was exhibited after exposure to air for 60 days. Although these reports demonstrated that Cu NPs could be capped with graphene layers, they were mainly formed by the coalescence of synthesized C/Cu nanoagglomerates during a collision process in the reaction atmospheres, which posed constraints on the controllability of size and shape of the Cu NPs.

Here, we demonstrate a facile process to fully encapsulate Cu NPs with few layers of graphene using a solid phase carbon source of poly(methyl methacrylate) (PMMA), leading to the fabrication of graphene nanoballs (GNBs) with Cu cores. Since the encapsulation process is performed on the separately prepared Cu NPs, our method can be generally applicable to encapsulation of Cu NPs with variable sizes and shapes. It was observed that when the carbon source was supplied in gas phase, the high temperature of the CVD process (800−900 °C) led to the agglomeration of the Cu NPs. Notably, the Cu NPs were not agglomerated after the same process using the solid carbon source of PMMA; few-layered graphene (FLG) could be directly synthesized on the Cu NPs, which was confirmed from the Raman analysis. The high-resolution transmission electron microscope (HR-TEM) micrographs verified that the Cu NPs were encapsulated with FLG. The results of X-ray diffraction and X-ray photoelectron spectroscopy analyses in combination with electrical resistance measurement with respect to temperature variation showed that the Cu NPs were highly resistant to oxidation after encapsulation with FLG.

2. EXPERIMENTAL SECTION

Figure 1 schematically illustrates the fabrication procedures of GNBs. Cu NPs used in this report were purchased from Sky Spring Nanomaterials (mean diameter of 500 nm, hereinafter referred as Cu500) and US Research Nanomaterials (mean diameter of 70 nm, Cu70). For the preparation of a solid carbon source, PMMA powder from Sigma Aldrich (average molar weight of ∼996 000, product no. 182265) was dissolved in a mixed solution of dimethylformamide and α-terpineol (8:2 volume ratio) with a concentration of 20 mg/mL. Then, 0.5 g of Cu500 and 0.1 g of Cu70 were separately mixed with 5 mL of the PMMA solution and stirred for 12 h using a magnetic bar. The mixed solution was drop-cast on cleaned Si substrates covered with a SiO_2 layer and cured at 110 °C for 10 min. The specimens were then loaded into a CVD quartz chamber. For synthesis of graphene layers, 50 sccm of H_2 and Ar gases each were supplied to the furnace and heated to the annealing temperature ranging from 800 to 900 °C at a total pressure of 0.7 Torr. The ramping rate of the temperature was approximately 60 °C/min during the heating process, followed by natural cooling to room temperature with an identical gas configuration as the annealing condition.

The morphologies of the Cu NPs and Cu-cored GNBs were characterized using a FE-SEM (JSM-7001F, JEOL Ltd.) and a HR-TEM (JEOL 3000F). For Cu500-cored GNBs, 200-nm-thick Al layer was evaporated on the top side of the samples to ensure that the Cu500-cored GNBs would not be detached during the mechanical milling for the TEM observation. On the other hand, Cu70-cored GNBs were collected using a blade and then placed on carbon mesh TEM grids. Raman spectra were obtained using a micro-Raman system (Jobin-Yvon, LabRaman HR) with a laser wavelength of 532 nm to confirm the synthesis of graphene layers on the Cu NPs. Specimens were immersed in 20% HNO_3 for 12 h followed by thorough rinsing in deionized water for 15 min before the Raman measurements. The surface chemistry of the GNBs was characterized using a combination of an XRD (Rigaku, D/Max-2500H) system equipped with a Cu Kα1 source (λ = 1.540562 Å) and an XPS (Thermo Scientific, K-alpha) system equipped with a monochromatic Al Kα source ($h\nu$ = 1486.6 eV). The normalized resistance of the Cu-cored GNBs was monitored using a Keithley 2400 SourceMeter while increasing the annealing temperature from 30−250 °C at a rate of 1 °C/min to observe the effect of copper oxidation on the conductance of the Cu-cored GNBs at different temperature regimes. To measure the electrical resistance, a simple device configuration having Cu-cored GNBs and Au pads as contacts was prepared by the following processes. First, Cu-cored GNB solution was prepared by immersing the synthesized into isopropyl alcohol, followed by a brief sonication. The Cu-cored GNB solution was then drop-casted on a 300-nm-thick SiO_2 substrate patterned with 50-nm-thick Au contacts separated by 200 μm.

3. RESULTS AND DISCUSSION

Figure 2a−c represent the typical SEM images of Cu500 prior to (Figure 2a) and after the GNB synthesis process at 900 °C using PMMA (Figure 2b) and methane gas (CH_4, Figure 2c) as carbon sources. The Cu500 NPs with diverse diameters ranging from 200 nm to 1 μm showed no significant morphological changes after the annealing step at 900 °C when PMMA coating was used as shown in Figures 2a and 2b. However, the Cu500 NPs were highly agglomerated to form clustered structures when CH_4 was used (Figure 2c). The agglomeration of Cu NPs during the CVD with a gas source can be attributed to the high annealing temperature that could reach to the melting temperature of Cu NPs; although the known melting temperature of Cu is approximately 1080 °C, the enhanced vapor pressure of the Cu surface atoms due to its nanoscale

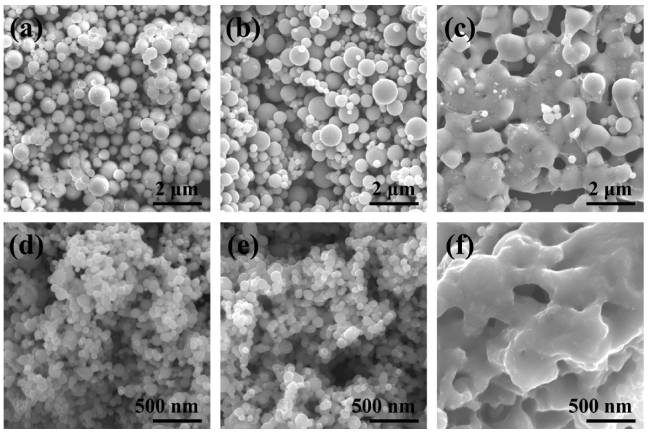

Figure 2. SEM images of Cu500 and Cu70 for (a, d) as-prepared NPs on SiO_2 substrates, (b, e) after graphene growth using solid carbon source, and (c, f) after same growth conditions using CH_4.

dimension resulted in the decrease of melting temperature, and Cu NPs were agglomerated to minimize the surface energy.[15] Similar results have been previously reported by Wang et al.,[16] where Cu nanowires were melted and formed irregular shapes after the CVD process using ethylene gas (C_2H_4) as precursor at 1,000 °C. On the contrary, the Cu NPs could be protected from morphological deformation by the formed carbon shells during the annealing procedure, which is known to grow on the surface of Cu from carbon source of PMMA at temperatures above 400 °C.[17]

Figures 2d-f show the SEM images of Cu70 prior to (Figure 2d) and after the GNB synthesis process at 800 °C using PMMA (Figure 2e) and CH_4 (Figure 2f) as carbon sources. When the size of the Cu NPs was reduced to below 100 nm, the Cu NPs were marginally agglomerated after the same growth condition (see Figure S1 in Supporting Information), which can be attributed to the larger surface area and increased vapor pressure of the smaller Cu NPs; to effectively separate and protect the Cu70, the PMMA/Cu mass ratio was increased from 0.2 to 1 while lowering the process temperature to 800 °C. As a result, Cu70 NPs could be fully encapsulated by graphene layers with no significant morphological change (Figure 2e) when PMMA coating was used. As expected, they were agglomerated when CH_4 was used (Figure 2f). It indicates that the use of a solid carbon source such as PMMA effectively preserved the original morphologies of the Cu NPs for the growth of graphene on the Cu NPs, which could be applicable to 40-nm-sized Cu NPs in our experimental range. To estimate the size range within which our technique can be applicable, the size-dependent melting point of Cu NPs was theoretically investigated; the Gibbs−Thomson equation was used to calculate the structural melting point depression[18] (see Figure S2 in the Supporting Information). According to the equation, the melting point of Cu NP reaches 800 °C when the size is reduced to approximately 2.7 nm. Considering that graphene can be grown on Cu using PMMA at 800 °C,[17] we anticipate that our fabrication method of Cu-cored GNBs could be applicable even for Cu NPs with sizes below 10 nm if the Cu NPs are well-separated and sufficient solid carbon source is supplied.

To verify the formation of graphene layers on the outer shell of Cu NPs, we performed Raman analysis. Prior to the Raman measurements, the Cu NPs were etched by immersing in HNO_3 for 12 h to avoid the overlapping of Cu fluorescence peaks with the typical peaks of graphene layers.[19] Figures 3a and 3b demonstrates the Raman spectra measured from Cu500-cored and Cu70-cored GNBs, respectively. The first-order region of both Raman spectra showed superpositioned D and G peaks with high intensity near 1360 cm^{-1} and 1590 cm^{-1}, respectively, and broad peaks were observed at 2300−3200 cm^{-1}. The high D peaks indicate the defective nature of the obtained graphene layers, which may have originated from the distorted hexagonal sp^2 carbon networks,[20] along with the strain-induced effects,[21,22] and finite particle-size effect;[14,23] because the carbon shells were synthesized on the spherical surface of the Cu NPs with radius ranging from 20 to 500 nm, the obtained structures resulted in very small domains, with their lattice considerably stressed because of the high curvature of Cu NP surfaces. Moreover, because the size of the laser beam used in the Raman measurements was approximately 1 μm, larger than the size of the Cu NPs, the contacted region between the GNBs could have been recognized as defects. Among these reasons, we assume that the D peak was mainly attributed to the structural effects and not to the actual defects in the graphitic lattice, and the detailed reasoning will be provided in the stability test results to oxidation.

The appearance of unusually shaped 2D peaks at 2300−3200 cm^{-1} can be explained by the nonplanar structure of GNBs. To better explain the reason for the broad 2D region, they were fitted using Lorentzian profiles and plotted in the insets of panels a and b in Figure 3. It was revealed that the broad region was composed of multiple peaks of 2D, D+G, and 2D′ at 2694, 2901, and 3085 cm^{-1} for Cu500-cored GNBs. The broad 2D region of Cu70-cored GNBs could also be divided into the same 2D, D+G, and 2D′ peaks at 2674, 2897, and 3085 cm^{-1},

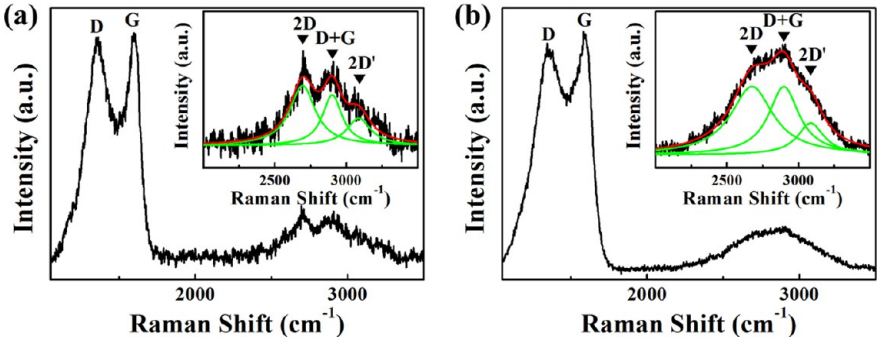

Figure 3. Raman spectra of (a) Cu500-cored GNBs and (b) Cu70-cored GNBs measured after removing Cu cores. The insets show the 2D region fitted using Lorentzian profiles.

dx.doi.org/10.1021/am3024965 | ACS Appl. Mater. Interfaces 2013, 5, 2432−2437

respectively. Such D+G and 2D′ peaks are not the typical peaks of planar graphene layers, but it has been previously reported that the D+G and 2D′ peaks arise in the Raman measurements of nonplanar graphitic layers, originated from the strained structure.[14,24,25] Thus, the presence of D+G and 2D′ peaks of the fabricated Cu500- and Cu70-cored GNBs can be explained since the graphene shells are directly synthesized on the surface of Cu NPs with high curvatures. The intensity ratio of the D+G to the 2D peak was higher for Cu70-cored GNBs (0.99) compared to that of the Cu500-cored GNBs (0.84), which can be ascribed to the higher curvature of the Cu70-cored GNBs.

Figure 4a is the typical low-resolution TEM micrograph of a Cu500-cored GNB. A Cu-cored GNB with diameter of approximately 800 nm was examined to analyze the detailed structure of the synthesized Cu500-cored GNBs. It is shown that the Cu NP retained its original shape even after the annealing process at the high temperature of 900 °C. From the high-resolution TEM image of Figure 4b, which was taken from the region enclosed with dotted rectangle in Figure 4a, it could be observed that FLG with thickness of ∼3 nm was directly formed on the surface of the Cu NP, corresponding to ∼8 layers of graphene. The lattice constant of the graphene layer was about 0.35 nm, which is comparable to the reported value of 0.34 nm.[26] Figure 4c is the typical low-resolution TEM micrograph of a morphologically preserved Cu70-cored GNB (70 nm in diameter). The thickness of the synthesized graphene layers observed from the high-resolution TEM image (Figure 4d) was ∼3 nm with 0.35 nm interlayer distance, also corresponding to ∼8 layers of graphene. The detailed growth mechanism of FLG on Cu NPs using PMMA carbon source can be explained as follows. First, the PMMA is dissolved at temperatures above ∼310 °C and a thin polymer film is formed on the Cu NPs, which is soon converted to a-C through a pyrolysis process at elevated temperatures over 400 °C.[27] The a-C layer works as a barrier that prevents the morphological change of the Cu NPs during the annealing process. Then, at annealing temperature of 800−900 °C, the a-C layers in direct contact with the Cu NPs are converted to FLG due to the catalytic effect of Cu,[17] whereas the formation of additional graphene layers were self-limited once FLG was formed on the surface of Cu NPs, restricting the catalytic effect of Cu by fully passivating the Cu NPs. This mechanism was quite different from that reported when a gas phase carbon source (i.e., CH_4) is used during the CVD synthesis of graphene on Cu:[28] it is known that a single-layer graphene is grown on the surface of Cu because of the low solubility of C atoms on Cu, which effectively passivates the surface of Cu and strongly obstructs the growth of multilayer graphene.[29]

Sun et al.[17] investigated the mechanism of PMMA conversion into graphene layers on Cu foils using thermal annealing at 1,000 °C. The thickness of the graphene layers could be controlled by varying the amount of H_2 gas flow during the annealing process; hydrogen has the role of both carrier gas and reducing reagent to eliminate C atoms which come from the decomposed PMMA during the annealing process. In their report, the increase of H_2 flow rate led to the reduction in the thickness of the obtained graphene layers, and when the rate of H_2 flow was low, multilayers of graphene were formed atop the first layer through graphitization of PMMA on the graphene lattice directly. This mechanism seems accurate considering the recent report of Lin et al.,[30] where FLG was directly grown on hexagonal boron nitride (*h*-BN) substrates by graphitization of PMMA on the lattice of *h*-BN, which is much similar to that of a graphene. Hence, it could be concluded that the abundance of carbon source resulted in the synthesis of additional graphene layers atop the first graphene layer on the spherical surfaces of Cu NPs by graphitization of PMMA.

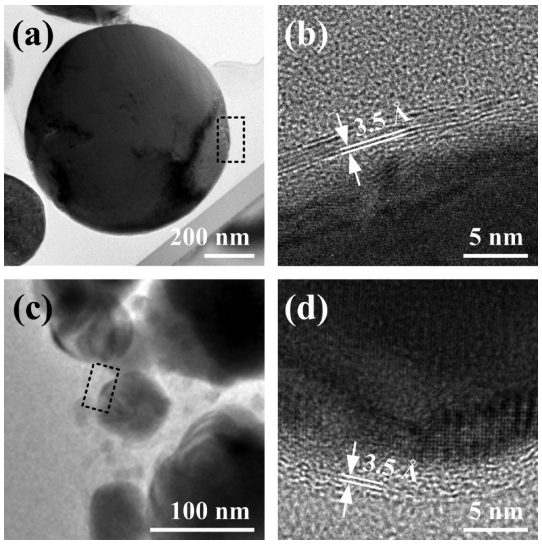

Figure 4. (a) Low-resolution TEM image of a Cu500-cored GNB, and (b) high-resolution TEM image of the region enclosed by dotted rectangle of (a) showing nearly 3-nm-thick graphene layers on Cu500-cored GNB. (c) Low-resolution TEM image of a Cu70-cored GNB, and (d) high-resolution TEM image of the region enclosed by dotted rectangle of c.

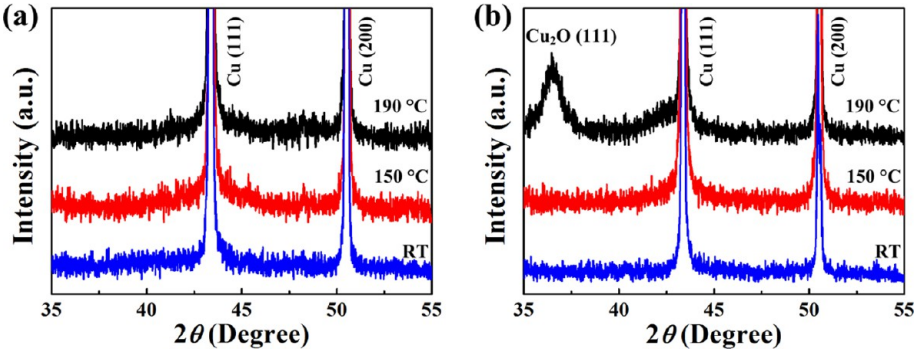

Figure 5. $\omega-2\theta$ scans of Cu-cored GNBs before and after annealing in air for 3 h for (a) Cu500-cored GNBs and (b) Cu70-cored GNBs.

dx.doi.org/10.1021/am3024965 | ACS Appl. Mater. Interfaces 2013, 5, 2432−2437

The stability of the synthesized Cu-cored GNBs under oxidation conditions was tested by annealing the Cu-cored GNBs up to 190 °C using a hot plate in ambient conditions for 3 h. Figure 5a shows the XRD ω-2θ scans of Cu500-cored GNBs under different annealing conditions of 150 and 190 °C, and at room temperature. The formation of copper oxides on the surface of bare Cu NPs is known to occur easily at room temperature within a few hours[5] through the following reactions: Cu (s) → Cu_2O (s) and Cu_2O (s) → CuO (s) (see Figure S3 in the Supporting Information). However, no sign of oxidation could be detected even after annealing the sample at 190 °C for 3 h, evidenced from the dominant Cu-related peaks at 43.3° (Cu (111)) and 50.5° (Cu (200)) and no appearance of copper oxide-related peaks. Thus, it can be inferred that the synthesized FLG well protected the Cu500 NPs from being oxidized. Figure 5b exhibits the XRD ω-2θ scans of Cu70-cored GNBs measured at room temperature and after annealing at 150 and 190 °C. The synthesized graphene layers well-protected the Cu70 NPs from oxidation at the annealing temperature of 150 °C, but a minor Cu oxide related peak of Cu_2O (111) was observed at 36.5° when the Cu70-cored GNBs were annealed at 190 °C. Chen et al. previously reported that the Cu located beneath the grain boundaries of graphene layers exhibited relatively poor oxidation resistances compared to the areas covered with nondefective graphene layers.[10] We suspect that the copper oxides could have been formed at the structurally vulnerable grain boundaries of the graphene shells formed on the considerably small-sized Cu NPs with sizes below 100 nm.

The detailed surface chemistry of the Cu-cored GNBs after annealing at 190 °C were characterized by the C1s peaks of the XPS measurements and plotted in Figure 6. Graphene is ideally

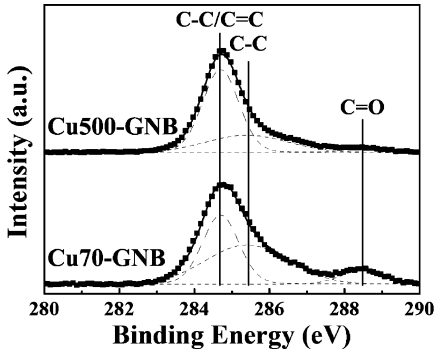

Figure 6. XPS spectra of C1s for Cu-cored GNBs after annealing at 190 °C for 3 h.

composed aromatic bonds (C−C/C═C) corresponding to sp^2-bonded carbon. Whereas the C═O bonds were rarely formed on the surfaces of Cu500-cored GNBs after annealing at 190 °C, it can be observed that the surfaces of Cu70-cored GNBs contained C═O bonds, which were probably formed at the grain boundaries of the Cu70-cored GNBs. Although the intensity of sp^2-bonded carbon peak is the highest, the C−C bonds corresponding to sp^3-bonded carbon at 285.4 eV has a higher intensity for Cu70-cored GNBs compared to that of Cu500-cored GNBs, indicating that the GNBs with smaller sizes and higher curvature are more defective.

Figure 7 illustrates the normalized electrical resistance of the Cu-cored GNBs measured while increasing the temperature from room temperature to 250 °C. In specific, the temperature

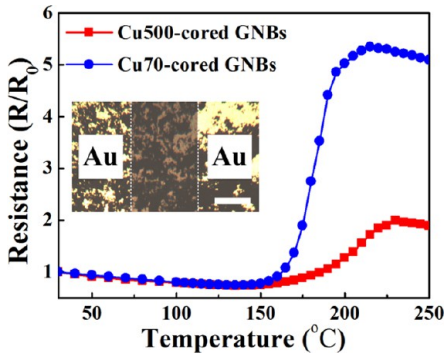

Figure 7. Normalized resistance of the Cu-cored GNBs measured as a function of temperature.

was increased at a rate of 1 °C/min and maintained at every 5 °C for 2 min to observe the change of the resistance. For both Cu500- and Cu70-cored GNBs, the normalized resistance maintains steadily until 150 °C, which is in good accordance with the XRD results. For Cu500-cored GNBs, the normalized resistance increased at higher temperatures above near 160 °C until it was doubled at approximately 230 °C and saturated thereafter. Although direct evidence of oxidation on Cu500-cored GNBs could not be observed in the XRD analysis, it can be inferred that the increase in the resistance of Cu500-cored GNBs was due to the oxidization at the relatively sparse grain boundaries of the GNBs and not by the failure of the graphene itself. In contrast, the normalized resistance of Cu70-cored GNBs sharply increased to approximately 5 times after increasing the temperature above 160 °C, which also gradually saturated after 230 °C. It also indicates that the graphene shells formed on the Cu70 NPs are more defective than those formed on Cu500 NPs, which is in a good agreement with the results of XRD and XPS analyses.

4. CONCLUSION

In summary, Cu-cored GNBs with variable sizes (from 40 nm to 1 μm) were synthesized without harming the original morphologies of the core Cu NPs using a solid carbon source of PMMA. TEM analysis confirmed that the synthesized graphene layers were approximately 3-nm-thick, which corresponded to few layers of graphene. The suggested growth mechanism of FLG on the surface of Cu NPs is as follows: first, PMMA was dissolved to form a thin polymer film on the Cu NPs at near 300 °C, which was soon converted into a-C layers above 400 °C, and finally converting into FLG by the catalytic effect of Cu. The synthesized FLG served as an excellent protector against oxidation at extreme conditions with only partial oxidation at the graphene grain boundaries, as confirmed by the XRD, XPS analyses, and electrical measurements. We expect that our method of fabricating GNBs can be applicable to other non-noble metal NPs.

■ ASSOCIATED CONTENT

Supporting Information

Further SEM images and plots for the Gibbs−Thomson equation. This material is available free of charge via the Internet at http://pubs.acs.org/.

AUTHOR INFORMATION

Corresponding Author

*Tel: +82-2-2123-5767. Fax: +82-2-313-2879. E-mail: taeyoon.lee@yonsei.ac.kr.

Notes

The authors declare no competing financial interest.

ACKNOWLEDGMENTS

This work was supported by the Industrial strategic technology development program (10041041, development of nonvacuum and nonlithography based 5 μm width Cu interconnect technology for TFT backplane) funded by the Ministry of Knowledge Economy(MKE, Korea)

REFERENCES

(1) Penn, S. G.; He, L.; Natan, M. J. *Curr. Opin. Chem. Biol.* **2003**, *7*, 609−615.
(2) Magdassi, S.; Bassa, A.; Vinetsky, Y.; Kamyshny, A. *Chem. Mater.* **2003**, *15*, 2208−2217.
(3) Chithrani, B. D.; Ghazani, A. A.; Chan, W. C. W. *Nano Lett.* **2006**, *6*, 662−668.
(4) Grunes, J.; Zhu, J.; Anderson, E. A.; Somorjai, G. A. *J. Phys. Chem. B* **2002**, *106*, 11463−11468.
(5) Liu, X.; Zhou, Y. *J. Mater. Res.* **2005**, *20*, 2371−2378.
(6) Magdassi, S.; Grouchko, M.; Kamyshny, A. *Materials* **2010**, *3*, 4626−4638.
(7) Rice, K. P.; Walker, E. J.; Stoykovich, M. P.; Saunders, A. E. *J. Phys. Chem. C* **2011**, *115*, 1793−1799.
(8) Karlsson, H. L.; Cronholm, P.; Gustafsson, J.; Möller, L. *Chem. Res. Toxicol.* **2008**, *21*, 1726−1732.
(9) Geim, A. K.; Novoselov, K. S. *Nat. Mater.* **2007**, *6*, 183−191.
(10) Chen, S.; Brown, L.; Levendorf, M.; Cai, W.; Ju, S.-Y.; Edgeworth, J.; Li, X.; Magnuson, C. W.; Velamakanni, A.; Piner, R. D.; Kang, J.; Park, J.; Ruoff, R. S. *ACS Nano* **2011**, *5*, 1321−1327.
(11) Bunch, J. S.; Verbridge, S. S.; Alden, J. S.; van der Zande, A. M.; Parpia, J. M.; Craighead, H. G.; McEuen, P. L. *Nano Lett.* **2008**, *8*, 2458−2462.
(12) Luechinger, N. A.; Athanassiou, E. K.; Stark, W. J. *Nanotechnology* **2008**, *19*, 445201.
(13) Athanassiou, E. K.; Grass, R. N.; Stark, W. J. *Nanotechnology* **2006**, *17*, 1668.
(14) Wang, S.; Huang, X.; He, Y.; Huang, H.; Wu, Y.; Hou, L.; Liu, X.; Yang, T.; Zou, J.; Huang, B. *Carbon* **2012**, *50*, 2119−2125.
(15) Nanda, K. K.; Maisels, A.; Kruis, F. E.; Fissan, H.; Stappert, S. *Phys. Rev. Lett.* **2003**, *91*, 106102.
(16) Wang, R.; Hao, Y.; Wang, Z.; Gong, H.; Thong, J. T. L. *Nano Lett.* **2010**, *10*, 4844−4850.
(17) Sun, Z.; Yan, Z.; Yao, J.; Beitler, E.; Zhu, Y.; Tour, J. M. *Nature* **2010**, *468*, 549−552.
(18) Jackson, C. L.; McKenna, G. B. *J. Chem. Phys.* **1990**, *93*, 9002−9011.
(19) Costa, S. D.; Righi, A.; Fantini, C.; Hao, Y.; Magnuson, C.; Colombo, L.; Ruoff, R. S.; Pimenta, M. A. *Solid State Commun.* **2012**, *152*, 1317−1320.
(20) Ferrari, A. C.; Meyer, J. C.; Scardaci, V.; Casiraghi, C.; Lazzeri, M.; Mauri, F.; Piscanec, S.; Jiang, D.; Novoselov, K. S.; Roth, S.; Geim, A. K. *Phys. Rev. Lett.* **2006**, *97*, 187401.
(21) Chen, Z.; Hong, G.; Wang, H.; Welsher, K.; Tabakman, S. M.; Sherlock, S. P.; Robinson, J. T.; Liang, Y.; Dai, H. *ACS Nano* **2012**, *6*, 1094−1101.
(22) Xiong, Y.; Xie, Y.; Li, Z.; Wu, C.; Zhang, R. *Chem. Commun.* **2003**, *9*, 904−905.
(23) Pimenta, M. A.; Dresselhaus, G.; Dresselhaus, M. S.; Cancado, L. G.; Jorio, A.; Saito, R. *Phys. Chem. Chem. Phys.* **2007**, *9*, 1276−1290.
(24) Tan, P.; Dimovski, S.; Gogotsi, Y. *Philos. Trans. R. Soc. London, Ser. A* **2004**, *362*, 2289−310.
(25) Kawashima, Y.; Katagiri, G. *Phys. Rev. B* **1995**, *52*, 10053−10059.
(26) Ishigami, M.; Chen, J. H.; Cullen, W. G.; Fuhrer, M. S.; Williams, E. D. *Nano Lett.* **2007**, *7*, 1643−1648.
(27) Byun, S.-J.; Lim, H.; Shin, G.-Y.; Han, T.-H.; Oh, S. H.; Ahn, J.-H.; Choi, H. C.; Lee, T.-W. *J. Phys. Chem. Lett.* **2011**, *2*, 493−497.
(28) Li, X.; Cai, W.; An, J.; Kim, S.; Nah, J.; Yang, D.; Piner, R.; Velamakanni, A.; Jung, I.; Tutuc, E.; Banerjee, S. K.; Colombo, L.; Ruoff, R. S. *Science* **2009**, *324*, 1312−1314.
(29) Li, X.; Cai, W.; Colombo, L.; Ruoff, R. S. *Nano Lett.* **2009**, *9*, 4268−4272.
(30) Lin, T.; Wang, Y.; Bi, H.; Wan, D.; Huang, F.; Xie, X.; Jiang, M. *J. Mater. Chem.* **2012**, *22*, 2859−2862.